Chapter

Mini Review: Recent Green Advances on the Preparation of V_2O_5, ZnO, and NiO Nanosheets

Daniel Likius, Ateeq Rahman, Elise Shilongo and Veikko Uahengo

Abstract

The past decade has seen a surge in the development of research on nanomaterial in the area of mixed metal oxides to fabricate ultrathin films, also known as nanosheets. In this review, different fabrication techniques of metal oxide nanosheets, such as vanadium, nickel, and zinc oxide, are presented. The chapter has also highlighted different ways of how to create smaller, affordable, lighter, and faster devices using vanadium, nickel, and zinc oxides. A detailed description of the synthesis and characterization using scanning electron microscope (SEM) and transmission electron microscope (TEM) for various shapes of nanomaterials is discussed in detail including factors that influence the orientation of nanosheets.

Keywords: nanosheets, nanoroses, nanoshapes, vanadium, nickel, zinc oxides

1. Introduction

Over the past decades, research efforts in nanoscience and nanotechnology has grown extensively globally due to the fabrication techniques of nanosheets that have attracted a great deal of research activities because of their unique physicochemical properties [1]. These properties have enabled scientists to be able to design and precise control over specialized morphologies of nanomaterials [2]. Consequently, the use of nanomaterials, the tremendous potential of "nano" approaches to revolutionize the ways in which matter is synthesized, fabricated and processed is already apparent. Currently, atoms, molecules, clusters and nanoparticles are used as functional and structural units for preparing advanced and totally new materials on the nanometer length scale [3–6]. The physicochemical properties of these nanomaterials usually depend on the meticulous property employed during the fabrication process: usually by changing the dimensions of the functional and structural units of the material as well as controlling their surface morphology, it is therefore possible to tailor functionalities in exceptional ways.

Moreover, the development of this multidisciplinary field was undoubtedly accelerated by the advent of relatively recent technologies that allow the visualization, design, characterization and manipulation of nanoscale systems. Generally, a nanosheet is a two-dimensional (2D) nanostructure with thickness in a scale ranging from 1 to 100 nm. Additionally, compare to other materials such as graphene, transition metal oxide nanosheets have attracted a lot of attention recently due to

their unique morphological advantages, and have shown a promising physicochemical properties for various applications. However, the fabrication of these transition metal oxide ultrafilms with controlled particles size and thickness remains a greater challenge for both fundamental study and applications. This chapter focuses on the synthesis of vanadium, nickel and zinc oxide nanosheets. The main basis for selecting these metal oxides chosen for investigation is based on the following highlights: vanadium (V), NiO, and ZnO are a highly abundant elements in the Earth's crust. Its oxides have been well known for multioxidation states (II–V) and various crystalline structures including VO_2, V_2O_5, and V_6O_{13}. Vanadium, NiO and ZnO exhibit excellent interactions with molecules or ions, outstanding catalytic activities, and/or strong electron–electron correlations [9–11].

Moreover, it also describes the morphological structures characterized by SEM and TEM techniques which include the demonstration on how these transition metal oxides change their morphology and tunable mesoporosity depend on the starting materials and heat treatment temperature.

2. Vanadium oxide nanosheets' preparation and characterization by SEM and TEM

Due to the chemical structure stability as well as the excellent physicochemical properties of vanadium oxides, these properties have attracted extensive attention for decades [7–10]. One of these vanadium oxides is vanadium pentoxide (V_2O_5) which is known as one of the best materials in nanotechnology study. Researchers have widely explored the V_2O_5 especially in alkali metal ion batteries [10]. Taking the inherent relationship between the microstructure and macroscopic properties in mind, the distinctive physicochemical properties can be synchronized and controlled via the approach of controllable synthesis of micro-/nanostructured materials. V_2O_5, nanosheets with various nanostructures such as nanosheets [11], nanoflowers [9], nanobelts [9], nanowires [8], nanoarrays, nanorods, nanobelts, nanonails, nanobridges, nanoprisms, nanotubes, nanobelts, nanorings, nanowhiskers, nanocombs, nanohelixes, nanosprings, nanopropeller, nanobows, nanocages, nanodisk, nanopoints, nanozigzag, nanostrings [9–11], and nanopores [8] have been fabricated. Moreover, the surface energy and surface defects of the active material are believed to contribute to the superior electrochemical performances has been developed and showed unique performances towards these specialized application. Peng et al. [11] reported V_2O_5 nanosheets with large area had been prepared via a freeze-drying process and following annealing treatment. In addition, the phase structure and morphology of V_2O_5 attained at different annealing temperatures was also systemically investigated. Xu et al. [12] reported the synthesis of V_2O_5 nanosheets by freeze drying method which uses hydrogen peroxide, freeze drying; post annealing and finally nanosheet can be obtained. The annealing temperature exhibited considerable influence on the microstructure of V_2O_5 nanosheets. V_2O_5 nanosheets obtained at annealing at different temperatures of 400, 450, 500 and 550°C exhibited comparatively in larger size, smaller thickness and smoother surface. **Figure 1** outlines the synthesis of V_2O_5 nanosheets as reported by Peng et al. [11].

Figure 2 shows the SEM images of V_2O_5 heat treatment at different temperature points reported by Xu et al. [12]. For V_2O_5 precursors in **Figure 2a**, layered particles are exhibited all over scattered the observed zoom. **Figure 2b** shows V_2O_5 annealed at 350°C with nanosheet microstructure with the transverse dimension greater than 10 μm and the thickness of less than 20 nm. As the heat treatment temperature increased to 400°C as shown in **Figure 2c**, the transverse dimension increased while the surface morphology became smoother. The thickness of V_2O_5 nanosheet increased

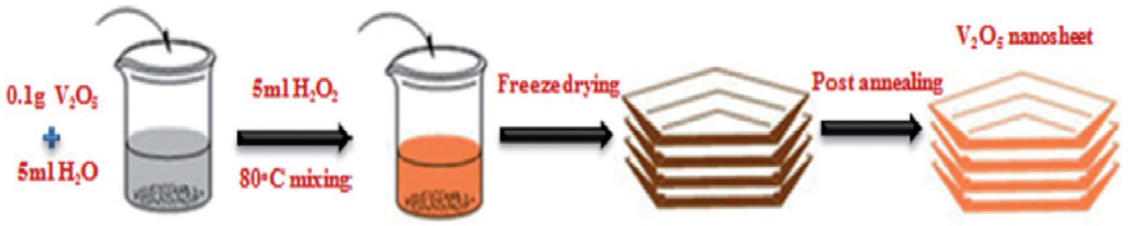

Figure 1.
Synthesis of V_2O_5 nanosheets by freeze drying method [11].

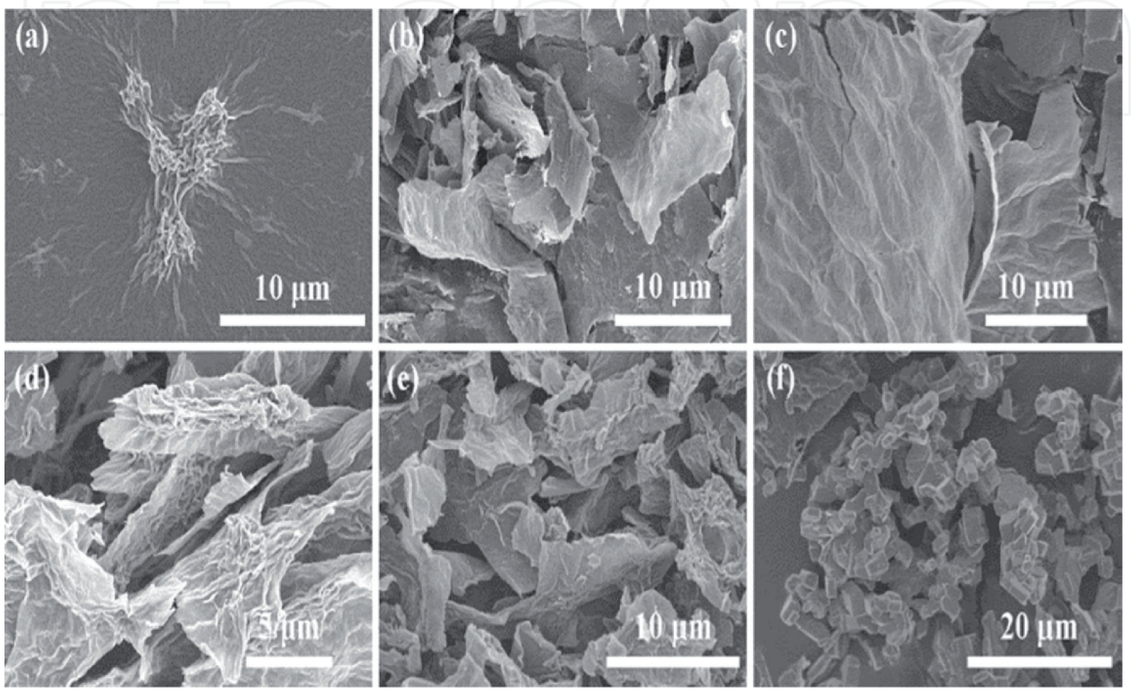

Figure 2.
SEM images of V_2O_5 nanosheet obtained at different temperature points: (a) V_2O_5 precursor, (b) 350°C, (c) 400°C, (d) 450°C, (e) 500°C, and (f) 550°C [11, 12].

by increasing the heat treatment temperature to 450°C (in **Figure 2d**) and some nanosheets gradually crumpled and agglomerated as the heat treatment temperature increased to 500°C (**Figure 2e**). The surface morphology of V_2O_5 heat treated at 550°C (**Figure 2f**) shows a mixture of agglomerated nanosheets and some regular polyhedral structures. The trend in the change of the morphological structures of V_2O_5 revealed that the heat treatment temperature possessed significant influence on the microstructure of V_2O_5. Finally, the V_2O_5 nanosheet heat treated at 400°C exhibited the optimal morphology with the largest size of transverse dimension and the thinnest thickness; hence 400°C is the optimal temperature for the fabrication of V_2O_5 nanosheet.

Liang et al. [13] reported the synthesis of vanadium nanosheets that the uniform V_2O_5 nanosheets were obtained by calcining the solvothermally prepared VO_2 nanosheets in air at 350°C for 2 h with a heating ramp of 1°C min^{-1}. Other scholars such as Cheng [14] also reported the synthesis of self-assembled V_2O_5 nanosheets/reduced graphene oxide (RGO) hierarchical nanocomposite nanosheet also using solvothermal method. In this nanocomposite, the V_2O_5 nanosheets assembling on the RGO constitutes a 3-D hierarchical nanostructure with high specific surface area and good electronic/ionic conducting path as shown in **Figure 3** [14].

The SEM images shown in **Figure 4** were obtained to study the morphology and the structure of the as-prepared V_2O_5 nanosheets/RGO hierarchical nanostructures [14]. As shown in **Figure 4a**, large 2-D free-standing nanosheets are observed. Similarly, it can be found from close examination from **Figure 4b** that the V_2O_5 nanosheets/

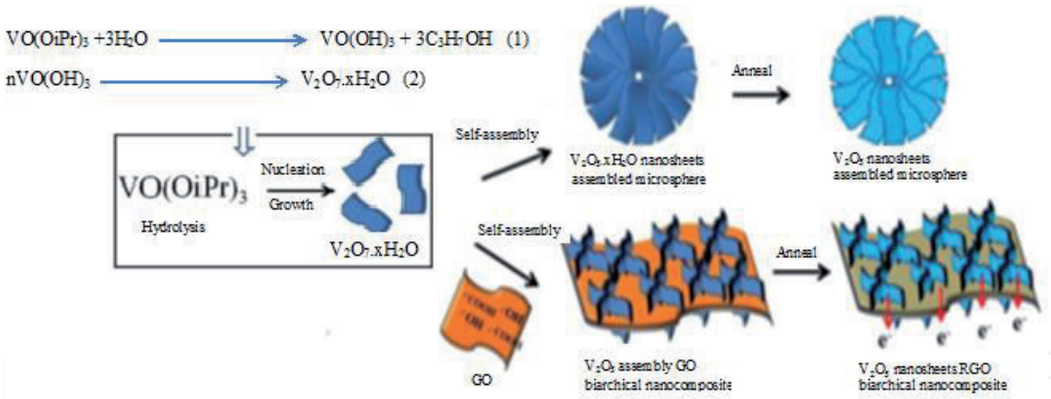

Figure 3.
Schematic illustration of the formation of 3-D V_2O_5 nanosheets/RGO hierarchical nanocomposite [14].

RGO nanocomposite is made up of multiple 2-D nanosheets on the surface of graphenenanosheets (GNS) [14]. Hence, without the addition of graphite oxide (GO), it is found that only 1-D lower-like V_2O_5 spheres consisting of many nanosheets are formed under the similar conditions. The TEM images in **Figure 5** shows that the V_2O_5 microspheres are composed of closely assembled nanosheets. Hence, by using GNS as the support, the formation of such a 3-D structure implies the effective growth of V_2O_5 nanosheets on the GNS. The structure can be further unraveled by element mapping images of carbon, vanadium and oxygen in the V_2O_5 nanosheets/RGO composite. It can be seen from **Figure 4c** that the carbon, vanadium and oxygen distributions are relatively uniform; carbon is also well dispersed all over the composites, suggesting the homogeneous dispersion of V_2O_5 on the GNS. TEM images in **Figure 5a** and **b** further show that the thin V_2O_5 nanosheets are uniformly distributed on the graphene sheets over a large area in the nanocomposite. The HR-TEM image in **Figure 5c** taken on an individual V_2O_5 nanosheet clearly shows crystal lattices with a d-spacing of 0.44 nm, corresponding to (001) planes of a crystalline orthorhombic phase of V_2O_5. The selected **Figure 5a** and **b** shows SEM images of V_2O_5 nanosheets/RGO hierarchical nanocomposite at different magnifications, respectively. The insert in **Figure 4a** shows a profile of a single nanocomposite sheet; **Figure 4c** shows SEM image of V_2O_5 nanosheets/RGO hierarchical nanocomposite with corresponding EDS maps of V, O and C elements (the Au is from sputter coating) [14].

Figure 6 presents field emission scanning electron microscopy (FE-SEM) and transmission electron microscopy (TEM) images of the V_2O_5 nanosheets/CNTs nanocomposite as reported by Wang et al. [14] using the freeze drying process. It is observed that V_2O_5 nanosheets and CNTs construct a uniform and homogeneous macro-morphology **Figure 6(a)**.

The carbon nanotubes (CNTs) act as "supporting-steel-like" architectures and the V_2O_5 nanosheets are anchored on the CNTs. They combine to form a highly porous structure as shown in **Figure 6b**. The TEM images in **Figure 6d** and **e** confirms that the V_2O_5 nanosheets and CNTs form a 3D interpenetrating of network structure. It is usually recognized that most nanosheets are easily overlapped and get bunched up to form bigger bulk due to the Ostwald ripening process, leading to the decrease of actually active surface and capacity loss for electrode materials [15]. In a study reported by Chen et al. [16], V_2O_5 nanosheets are anchored on the surface of CNTs without an overlap phenomenon. As the addition ratio of CNTs increases from 0 to 20 wt%, the morphology of the V_2O_5 nanosheets/CNTs nanocomposite becomes much more homogenous and the size of the V_2O_5 nanosheets becomes much smaller. The mechanism behind the formation of the 1D and 2D nanostructures can be explained in such a way that the functional groups on the CNT

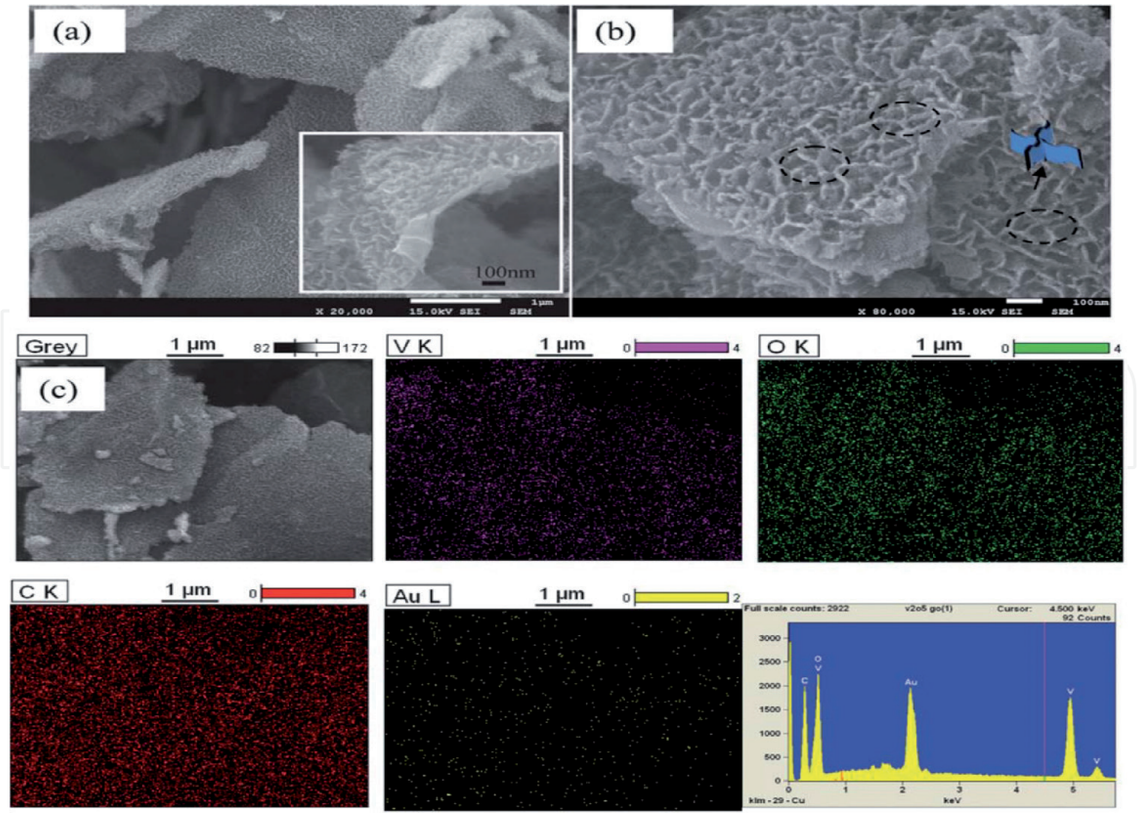

Figure 4.
(a and b) SEM images of V_2O_5 nanosheets/RGO hierarchical nanocomposite at different magnifications. The inset in (a) shows a profile of a single nanocomposite sheet; (c) SEM image of V_2O_5 nanosheets/RGO hierarchical nanocomposite with corresponding EDS maps of V, O and C elements (the Au is from sputter coating) [14].

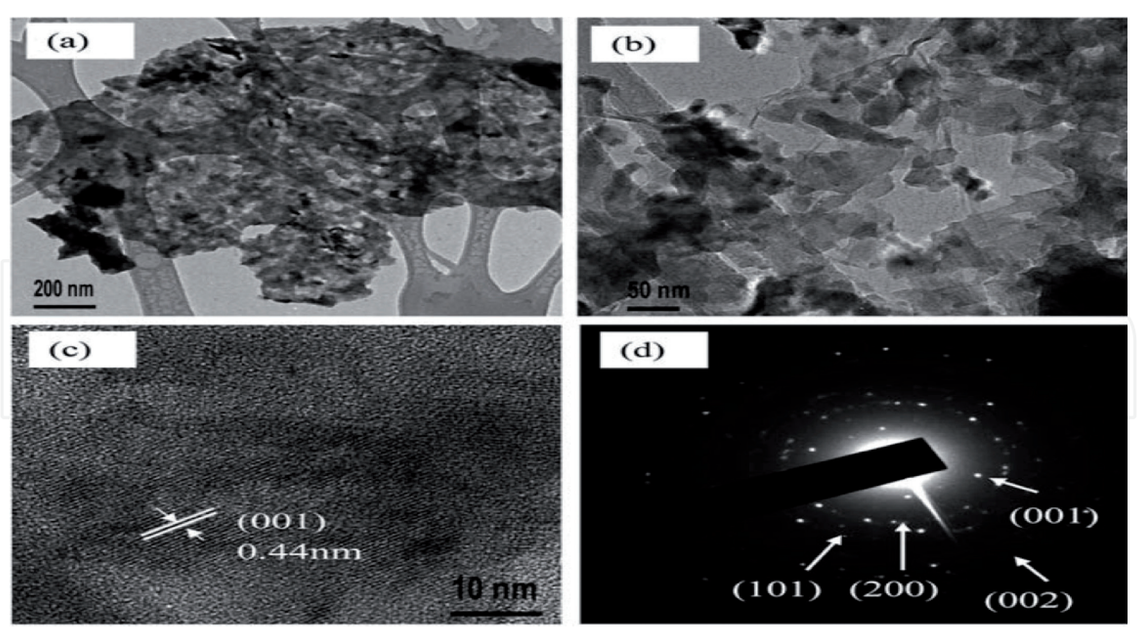

Figure 5.
(a and b) TEM images of V_2O_5 nanosheets/RGO nanocomposite at different magnifications; (c) HR-TEM image of V_2O_5 nanosheets/RGO nanocomposite; and (d) selected area electron diffraction (SAED) pattern [14].

surface act as the reaction centers. When the CNTs added into the vanadium oxide precursor solution, the vanadium oxytriisopropoxides bonded to the surface of the functional groups of CNT involved the electrostatic interaction bonding. During the freeze drying process, the hydrates in the V_2O_5 sol are frozen and removed [16].

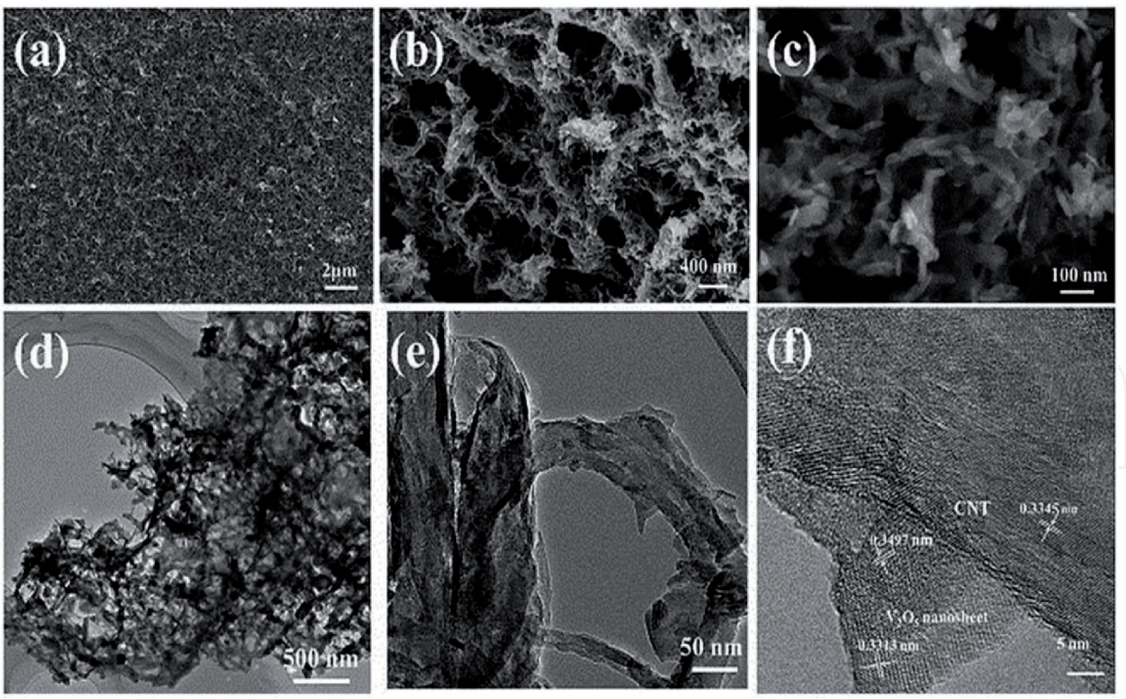

Figure 6.
The morphology observation of the V_2O_5 nanosheets/CNTs nanocomposite. (a), (b) low- and (c) high-magnification FESEM images; (d), (e) TEM and (f) HRTEM images [14].

3. Nickel oxide nanosheets preparation and characterization by SEM and TEM

Nickel (II) oxide (NiO) and nickel (II) composites in meticulously have attracted substantial interest because of a broad range of applications, namely magnetic materials [17], photovoltaic [18] Li ion batteries [19], catalysis [20], gas sensors [21], p-type transparent conducting films, infrared detectors, storage oxygen materials, fuels cells, supercapacitors, ferromagnetic oxides, gas sensors and luminescence materials, photochromic materials, [22], electrochromic windows [23], biomedicine, desalination, waste water treatment, energy related fields, catalytic reduction, adsorption, photocatalytic reduction, degradation, magnetic material, reinforcing agents in composites [24, 25]. Different methods have been reported for the synthesis of NiO, such as sol–gel [26], microemulsion [27], hydrothermal [28], co-precipitation, precipitation [29], sonochemical [15], microwave [30], metal–organic chemical vapor deposition (MOCVD), sputtering method [30], pulsed laser deposition (PLD), infrared irradiation, thermal decomposition, thermal evaporation and condensation [29, 30].

Nickel oxide is a predominantly interesting oxide because of its chemical and magnetic properties. There are various potential attractive applications of NiO in a variety of fields, such as absorbents, catalysis, battery cathodes, gas sensors, electrochromic films, magnetic materials, active optical fibers and fuel cell electrodes [31, 32]. The best know method for the fabrication of NiO nanosheets is through thermal decomposition of either nickel salts or nickel hydroxides. During this process the organic or halides on nickels burned which results in inhomogeneity of morphology and crystallite size of nickel oxide. Many efforts have been exerted to prepare NiO possessing controlled these inhomogeneity of morphology and crystallite size [33–36]. Although morphologically controlled synthesis of NiO nanocatalyst is becoming very much significant for catalytic reactions. These materials showed good electrochemical performance because of their special structure [37–41]. The fundamental process usually depends on the liquid-phase growth

of ultrathin lamellar nickel hydroxide precursor under microwave irradiation as reported by Chen et al. [16]. Using urea (NH_3), during this stage, the reactions experience a homogeneous alkalinization of nickel (II) nitrate. This is followed by the hydrolysis of sodium hydroxide (NaOH) using inductive effect provided by microwave irradiation at low-temperature condition. The setup of the microwave reactor with a three-necked flask experiment is illustrated in **Figure 7a**. The optimal thermodynamic and kinetic factors are important parameters to control for the growth of ultrathin intermediate [41, 42]. The formation of nanosheets is dominated by a self-assembly and oriented attachment mechanism. The swift microwave heating allows the best saturation of reactant species for 2D anisotropic, which causes a quick formation of ultrafine nanocrystals and then spontaneous self-assembling facilitated by natural driving force of lamellar nickel hydroxide. The α-$Ni(OH)_2$ nanosheets can be totally decomposed in to NiO when annealed at 300°C (**Figure 7b-d**).

It is well noted that water molecule is a crucial reaction parameter in the fabrication of NiO nanosheet [42] (**Table 1**). In the presence of light amount of water molecules in the reactor, NiO samples are able to gain self-supporting mechanism and also exhibit a large area sheet-like morphology. However, when the amount of water decreased in the reactor, the product aggregated and became a flower-like quasi-spherical 3D hierarchical structure as shown in **Figure 8a**. It was however, observed that, they do regain their sheet-like building blocks as the water molecules removed (**Figure 8b**). In the total absence of water, the NiO surface morphology turned into spherical aggregates (**Figure 8c**) causing the disappearance of nanosheets arrangement.

Baghbanzadeh et al. [42] is in agreement with the above statements as they reported that the current methodology demonstrates that directional hydrophobic attraction plays essential role in determining morphologies of final products. There are two factors that influence the formation of nanosheet during microwave irradiation to assist liquid-phase growth procedure. The first factor is the layered-structural nature and the second factor is the hydrophobicity. As mentioned above, the 2D anisotropic growth of nanosheets need a large driving force, thus it is possible for them to grow into nanolayer to form layered crystals. This is achieved due to the intrinsic driving force provided by lamellar $Ni(OH)_2$

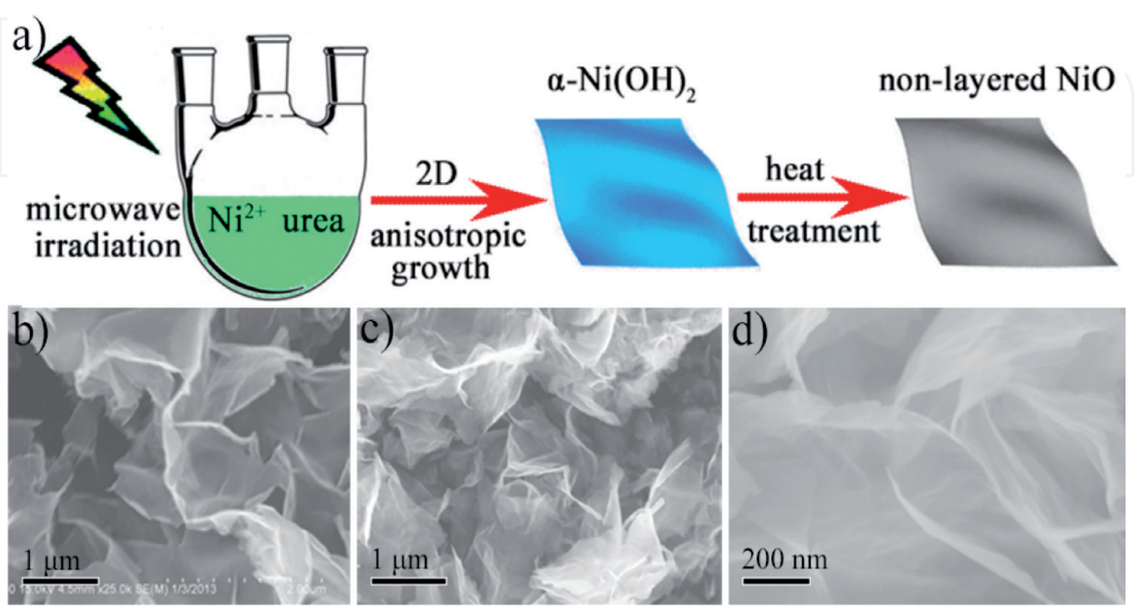

Figure 7.
(a) Schematic illustrating synthesis of nanosheets; FESEM images of (b) a-$Ni(OH)_2$ and (c), (d) NiO nanosheets [41, 42].

S. No.	Nanostructures	Particle size	Methods/conditions	Figure/ Reference
1.	V_2O_5 nanosheets	10–20 μm	Freeze drying 80°C, mixing	1–2/[1]
2.	V_2O_5 nanosheets RGO hierarchal nanocomposite	1 μm	a. Hydrothermal b. Condensation c. Nucleation calcination 350°C 2 h	3/[14]
3.	NiO nanolayered	200 nm 1 μm 20 μm	a. Microwave irradiation b. A-$Ni(OH)_2$ 2D anisotropic growth c. Heat treatment	7/[41, 42] 5/[14]
4.	NiO flower flake architecture	2 μm, 1 μm, 500 nm	SDS assisted self-nucleation assembly growth 6, 9, 12 h	10/[45]
5.	Needle-like NiO nanosheets	2 μm, 10 μm, 1 μm	a. Complexation b. Aggregation c. Fabrication	12/[46]
6.	ZnO nanosheets	200 μm, 3 μm, 500 nm	Preheating by hydrothermal method 0–24 h	14/[48] 15/[48]

Table 1.
Nanostructures of different fabrication techniques.

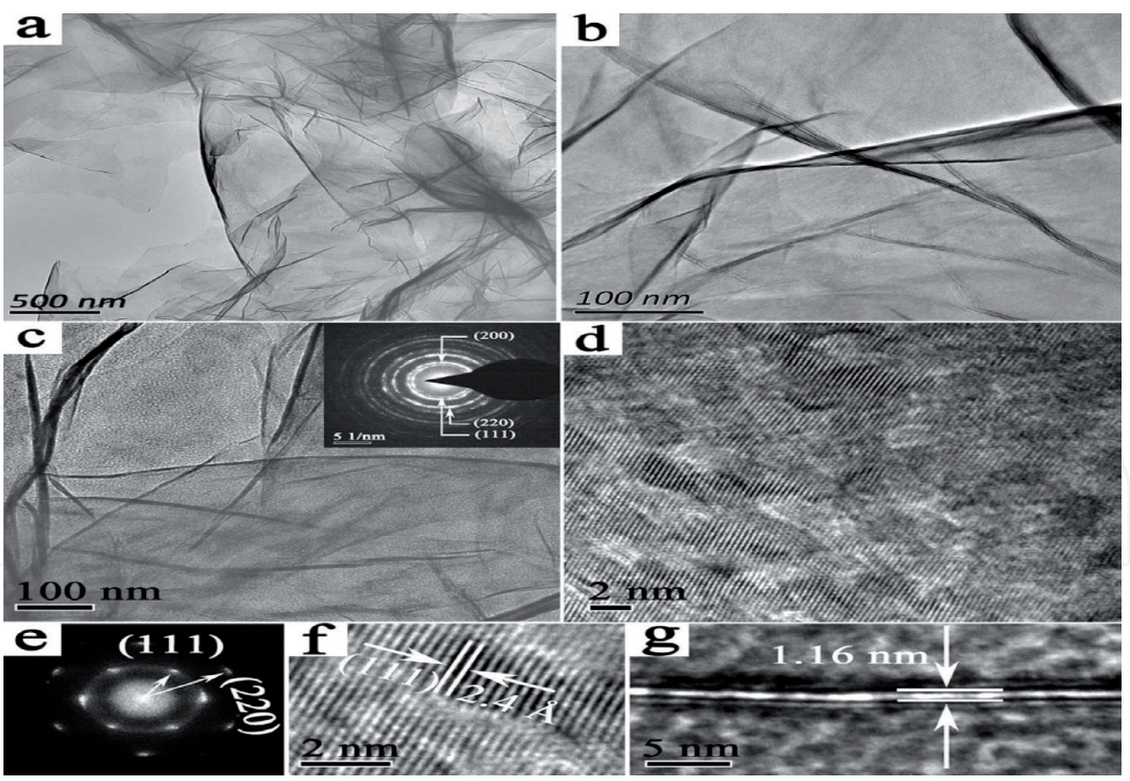

Figure 8.
(a) Low and (b) high magnification FESEM images of a-$Ni(OH)_2$ nanosheets; (c) TEM image (the inset showing SAED pattern), (d) a planar HRTEM image, (e), (f) the corresponding FFT pattern and enlarged HRTEM image recorded from (d), and (g) a vertical HRTEM image of NiO nanosheets [41, 42].

which is enough for the 2D anisotropic growth under microwave irradiation. From this, one can tell that layered-structure is a necessary requirement for the formation of 2D morphology.

As mentioned above, hydrophobicity is also one of the factors that influence the formation of nanosheet. The hydrophobicity is necessary to bring about the directional hydrophobic attraction between nanocrystals and water molecules, and it forms two phases that interface where the excessive surface energy can be accommodated [42]. There must be a balance of anisotropic hydrophobic attraction and electrostatic interaction for the spontaneous attraction of nanocrystals in order for nanosheets to be formed [43, 44]. This interaction is important to prevent their potential of shrinking and aggregating, hence allow the epitaxial orientation of the crystals. This means that the presence of the hydrophobicity terminate their stacking and packing, leading to ultrathin 2D structure rather than 3D graphite-like layered framework.

Weng et al. [45] reported the synthesis of NiO nanoflowers by hydrothermal process. **Figure 9** shows the SEM images of as-synthesized NiO. **Figure 9a** and **b** illustrates the novel hierarchical flower-like structure of the sample, which has a high similarity with the natural peony flower (inset). In **Figure 9c**, the enlarged patterns evidently exhibit that the formation of these flake-flower architectures is attributed to the partial overlapping of numerous irregular-shape ultrathin nanosheets with a thickness of approximately 10–20 nm, which are closely packed and form a multilayered structure [45].

Weng et al. [45] further reported the growth mechanism of SDS-assisted self-assembly and transformation mechanism for the synthesis of NiO flake-flower architectures. This was projected on the basis of the experimental observations and analysis reported by Zhang et al. [44] by preparation method using hydrothermal process whereby nickel chloride hexahydrate and urea served as nickel source and precipitant, respectively. The reactions with the formation proceeding are shown in Eqs. [44]:

$$CO(NH_2)_2 + 3H_2O \rightarrow 2NH_3\,H_2O + CO_2 \quad (1)$$

$$NH_3\,H_2O \rightarrow NH^{4+} + OH^- \quad (2)$$

$$CO_2 + 2OH^- \rightarrow CO^{2-}{}_3 + H_2O \quad (3)$$

$$3Ni^{2+} + 4OH^- + CO_2{}^{3-} + 4H_2O \rightarrow Ni_3(CO_3)(OH)_4 \cdot 4H_2O \quad (4)$$

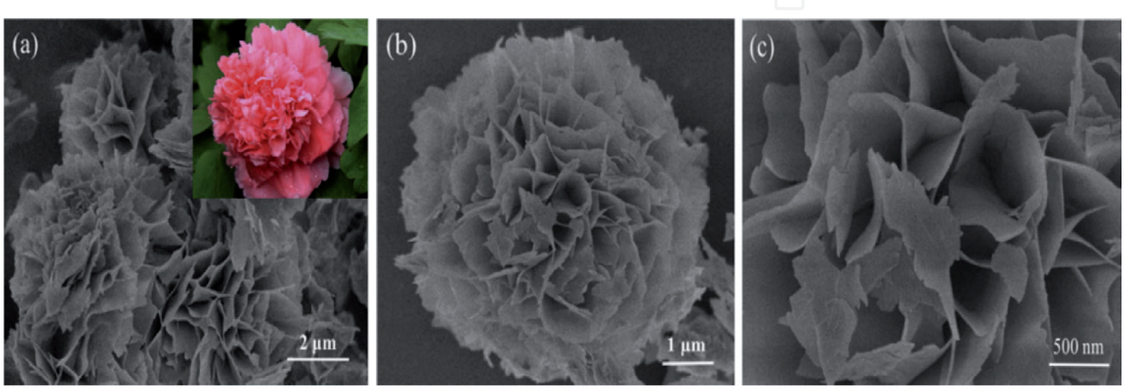

Figure 9.
(a)–(c) SEM images of the final hierarchical NiO flake-flower architectures [45].

$$Ni_3(CO_3)(OH)_4 \cdot 4H_2O \rightarrow 3NiO + CO_2 + 6H_2O \quad (5)$$

In the initial stage, the urea in aqueous solution began to hydrolyze and release ammonia, OH^- anions as well as CO_2^{3-} anions according to Eqs. (1)–(3). The Ni^{2+}

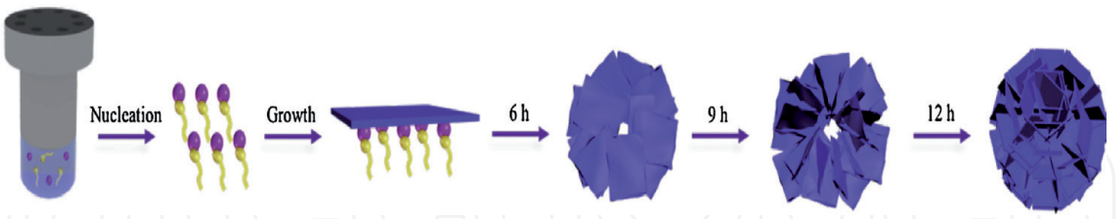

Figure 10.
Plausible SDS-assisted self-assembly and transformation mechanism for the synthesis of NiO flake-flower architectures [45].

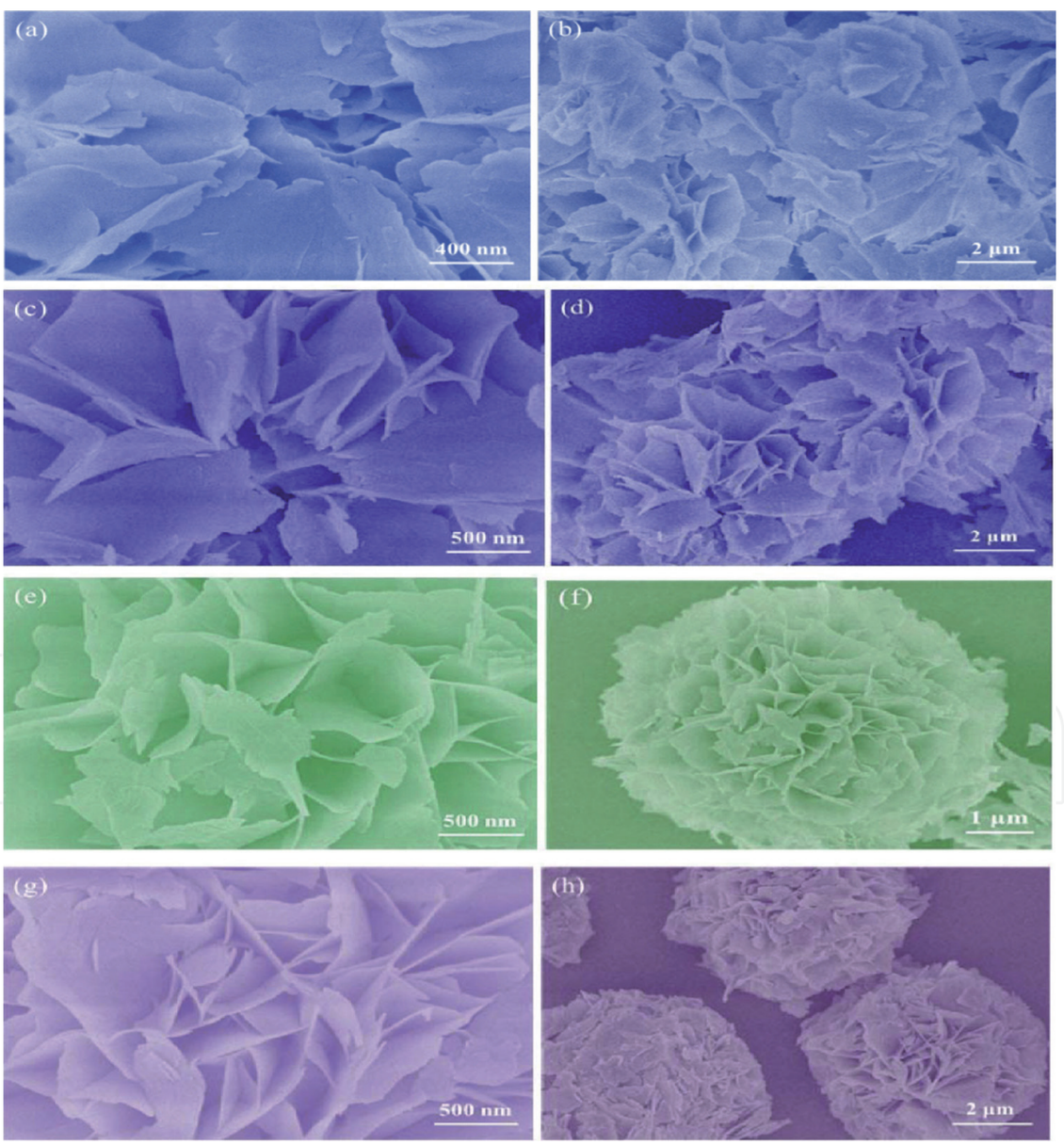

Figure 11.
(a) and (b) SEM images of NiO samples obtained at 160°C for 6 h. (c) and (d) SEM images of NiO samples obtained at 160°C for 9 h. (e)–(f) SEM images of NiO samples obtained at 160°C for 12 h. (g) and (h) SEM images of NiO samples obtained at 160°C for 15 h [45].

species then reacted with OH^- and CO_2^{3-} ions to produce nickel carbonate as shown in Eq. (4). By increasing the temperature and the pH value of the solution in Eq. (5), tiny single crystals nucleated steadily due to the thermodynamic and dynamic effects [16]. With time, these tiny homogeneously nucleated crystals started to aggregate to form nanosheets through spontaneous self-organization of neighboring particles aiming to have an identical crystal orientation at the planar interface, process known as oriented attachment [31]. During oriented attachment, SDS, which is an ionic surfactant, temporarily, acted also both as a structure-directing agent as well as a capping agent in the development of aggregation and enhancing absorption on the surface of the tiny crystals, respectively, in order to reduce the superficial area and their energy as illustrated in **Figure 10** [45]. However, long-chain alkyl groups from SDS produced external steric repulsion against the van der Waals attractive force so that the particles do not aggregate excessively [33, 34], which contributed to the ultra-thin nanosheets. **Figure 11** shows the SEM images of NiO nanosheets produced at the same heat treat temperature but at different annealing time.

Wen et al. [46] reported the synthesis of needle shaped NiO nanosheets by hydrothermal process as presented in **Figure 12**. The surface structures of both precursor ($NiC_2O_4.2H_2O$, (EG)) and final products (NiO) were characterized by FE-SEM observations. **Figure 13** shows the needle-like and flower-like structures of $NiC_2O_4.2H_2O$ produced by varying amount of sodium oxalate [46]. The needle-like $NiC_2O_4.2H_2O$ structures in **Figure 13a** were synthesized by using 0.061 g Sodium oxalate. By decreasing the amount of sodium oxalate to 0.022 g, the nanoflowers of $NiC_2O_4.H_2O$ were generated as shown in **Figure 2b** [46].

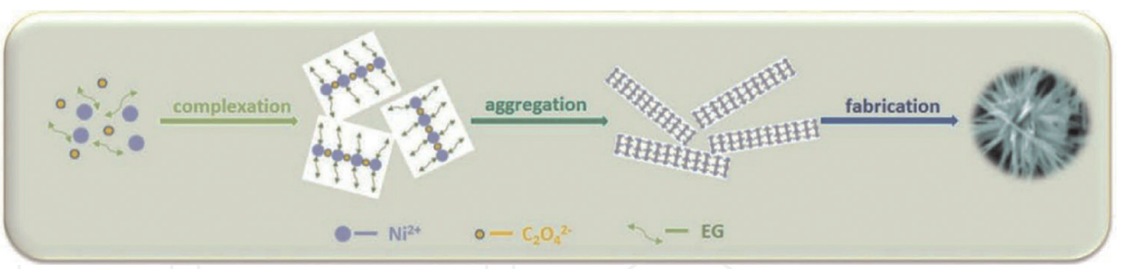

Figure 12.
Synthesis of needle-like NiO nanosheets [46].

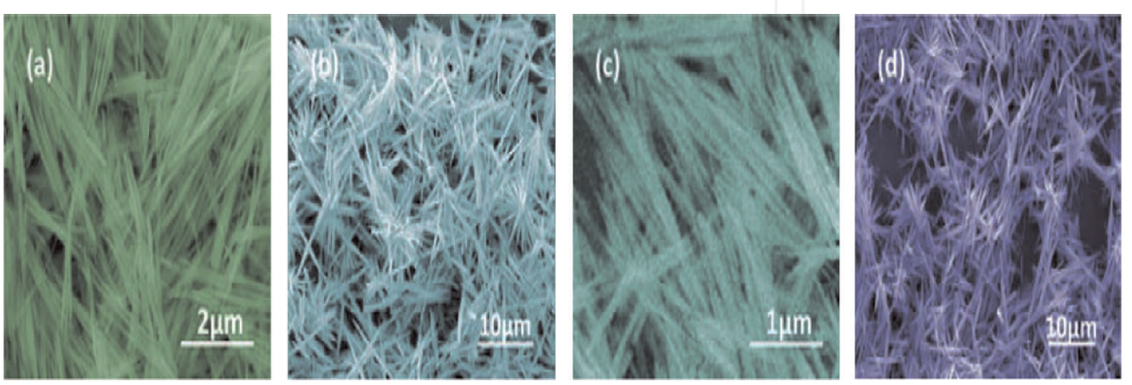

Figure 13.
SEM images of the $NiC_2O_4.2H_2O$ and NiO: (a) and (c): needle-like architectures; (b) and (d): needle-flower architectures [46, 47].

4. Zinc oxide nanosheets preparation and morphology study by SEM and TEM

Wang et al. reported [48] the synthesis of ZnO nanostructures using a surfactant-free hydrothermal method. A schematic growth diagram of the ZnO nanostructures fabricated by preheating hydrothermal method is shown in **Figure 14**.

The morphology of the as-grown flower-like ZnO architectures were then investigated by field-emission scan electron microscopy (FE-SEM) and the results are shown in **Figure 15**.

The SEM image shown in **Figure 15(a)** demonstrates that the sample obtained after preheating for 12 h have high density flower-like ZnO architectures uniformly grow and extremely disperse in the substrates without any aggregation, with specifying high yield and good uniformity accomplished with this fabrication condition [48]. The middle magnification FE-SEM image in **Figure 15(b)** confirms that individual flowers has a diameter of about 40–50 μm and consists of hundreds of thin curved nanosheets, which are spoke wise, projected from a common central zone. As presented in **Figures 15(c)** and **(d)**, high magnification FE-SEM image reveals that these ZnO nanosheets produced with the shape of flower-like architectures. The white squares in **Figure 15(e)** represent the low density ZnO nanorods which can be seen on the space without flower-like ZnO. The shape of ZnO nanorods were found to be hexagonal prism with a pyramidal top and smooth side surface and the majority of the ZnO nanorods are perpendicular to the ZnO supportive substrate. This was proved by increasing the magnification of the SEM image as shown in **Figure 15(f)**.

Wang et al. [48] also reported on the shapes of ZnO architectures removed from their supportive substrates using TEM images as shown in **Figure 16**.

The TEM images proved that the fabricated ZnO nanorods are made up of projected thin nanosheets as represented in **Figure 15a** [46, 47]. These ZnO nanosheets were found to be thin and have flat surfaces as shown in **Figure 15b**. Two sets of well resolved parallel lattice fringes are observed in high resolution TEM in **Figure 15c** [47]. The interplanar spacing is corresponding to that of {0002}

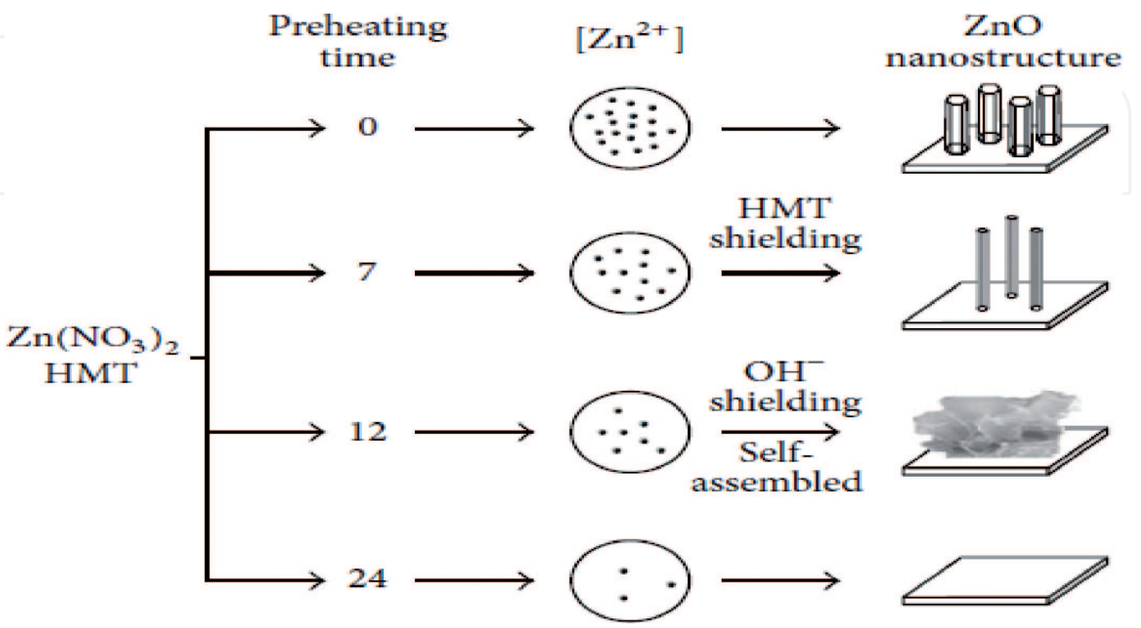

Figure 14.
Schematic growth diagram of the ZnO nanostructures fabricated by preheating hydrothermal method [48].

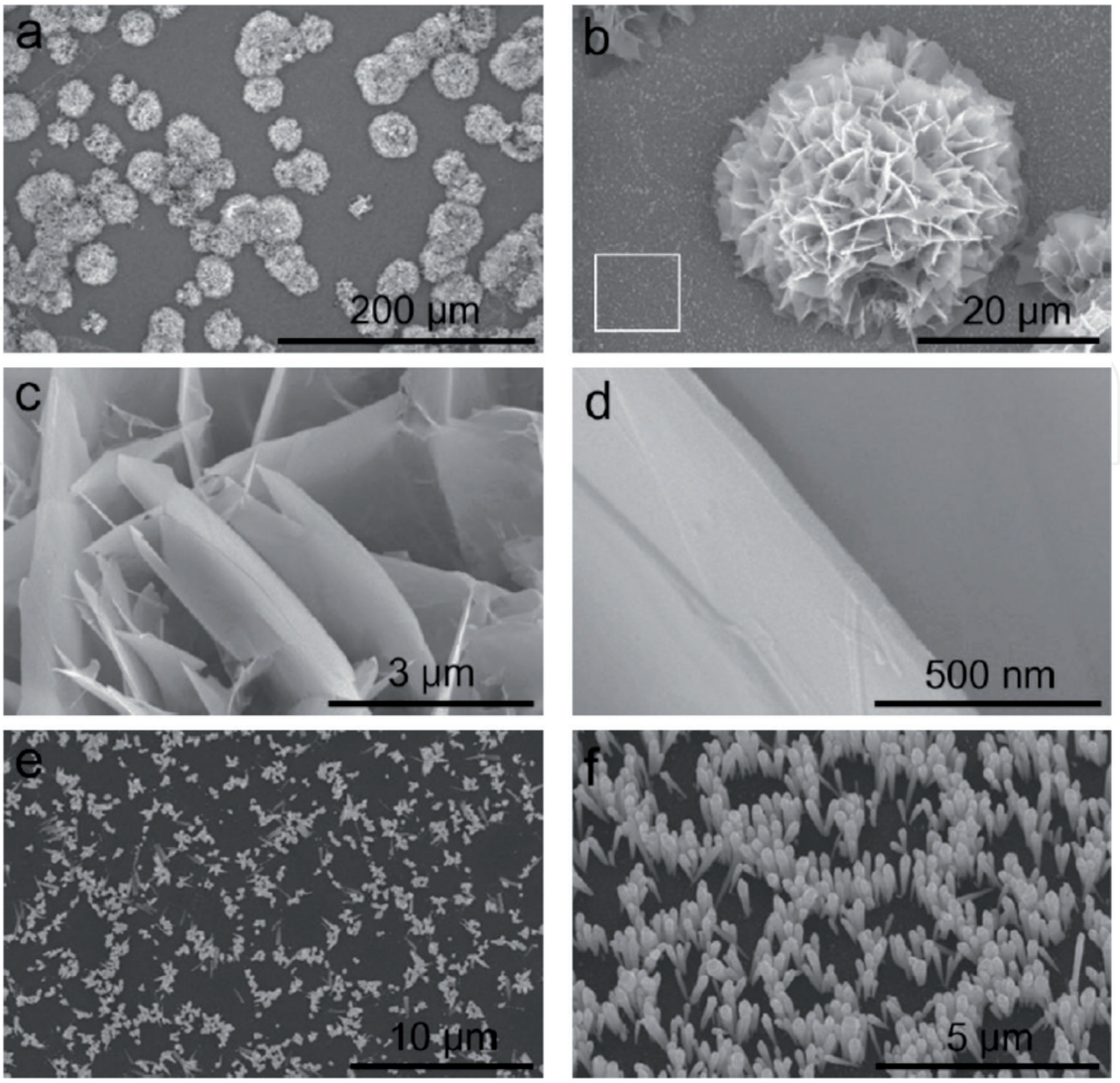

Figure 15.
FESEM images of flower-like ZnO architectures grown on ZnO thin film coated glass substrates. (a) Low magnification, (b) middle magnification, (c) and (d) high magnification of FESEM images of ZnO flowers, and (e) and (f) middle magnification of FESEM images from the space without ZnO flower, as indicated by the white square in (b) [48].

and {01–10} planes of ZnO crystals. **Figure 15d** is its SAED pattern and exhibits visible bright spots identical to all the crystal planes of the wurtzite ZnO, indicating a single crystalline with a good crystal quality. Based on HRTEM and SAED results, Wang et al. [49] suggested that the single crystal wurtzite ZnO nanosheet grows along [0001] and [01–10] crystallographic directions within the (2–1–10) plane. Hence, the flower-like ZnO growth process is summarized in **Figure 14**. Wang et al. [49] reported on study, Zn^{2+} and OH^- are provided by hydration of $Zn(NO_3)_2$ and HMT respectively. Therefore, the key chemical reactions can be formulated as shown in Eqs. (6)–(9):

$$(CH_2)_6N_4 + H_2O + \text{Heat} \rightarrow 4NH_{3(g)} + 6HCHO_{(g)} \quad (6)$$

$$NH_3 + H_2O \rightarrow NH_4^+ + OH^- \quad (7)$$

$$Zn_{2+} + 2OH^- \rightarrow Zn(OH)_{2(s)} \quad (8)$$

$$Zn(OH)_2 \rightarrow ZnO_{(s)} + H_2O \quad (9)$$

Wang et al. [49] have reported that in order to produce flower-like crystals of ZnO nanosheet also known as ZnO nanoroses, sodium citrate must be added in the reaction to create uniformity in the synthesis. Usually, cathodic electrodeposition is employed for the growth on polycrystalline ZnO thin films of different morphological orientation range from 1D (nanorods), 2D (nanoplates) to 3D crystals. However, Illy et al. [50] reported that the 2D sheet only found to occur when 1D sheets are allowed to combine under specific electrochemical conditions. **Figure 17** represents star-like and flower-like ZnO crystals. There is a big

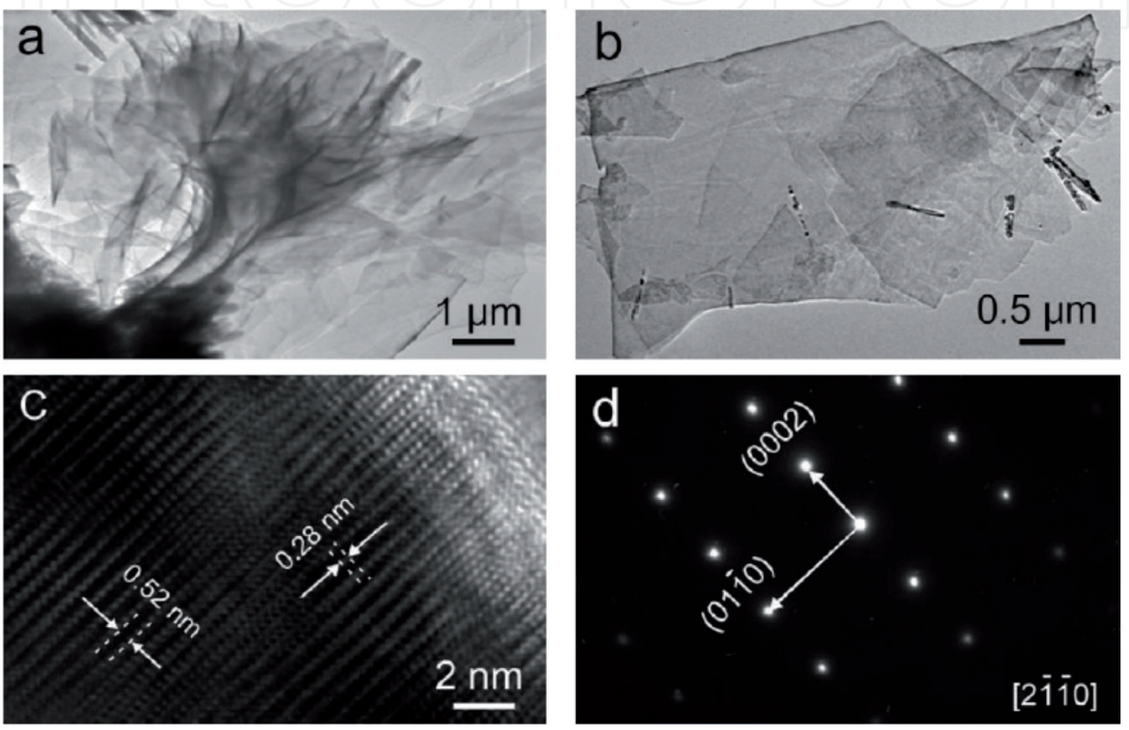

Figure 16.
TEM images of flower-like ZnO architectures. Typical TEM images of (a) an individual ZnO flower and (b) a piece of ZnO nanosheet. (c) HRTEM image and (d) SAED image of a piece of ZnO nanosheet [48].

Figure 17.
SEM images of the ZnO star-like crystals [50].

variation regarding the shape and morphology of the ZnO crystals shown. The nature and number of the reactants involved, the secondary products, concentration as well as complex ions in the solution are the main factors that contribute to the kinetics of the crystal growth [50]. With regard to concentration, Illy et al. [50] demonstrated that in order to produce the ZnO stars-like crystals, the concentration of $(CH_2)_6N_4$ must be in a 1 order of magnitude higher than $Zn(NO_3)_2{\cdot}6H_2O$. In terms of secondary products as an important factor, it was found that the production of an excess of oxygen containing species in solution increased competition for the interaction with a limited number of Zinc ions. One would expect then a reduction in the size of the ZnO rods compared to those hydrothermally formed from an equimolar reactant solution. Hence, these methods of synthesizing different shapes of nanomaterials exhibit quite remarkable properties.

5. Conclusion

This review highlighted the fabrication and characterization of various shapes of metal oxide nanosheets which are characterized by SEM and TEM instruments. Over the past decade, there has been enormous development of research on nanosheets, in the area of metal oxides. This offers basically new capabilities to architect a broad array of novel materials in the area of metal oxides and structures on a molecular scale. This chapter summarizes different ways to create smaller, cheaper, lighter and faster devices using vanadium, nickel, and zinc oxides. Structurally controlled synthesis at large of these nanomaterials can be attained morphologically nanomaterials would have the same importance for as controlling the helical angle of carbon nanotubes which determines it applications. These materials have remarkable applications in the all the branches of science, engineering and medicine in semiconductor, electronics, biomedicine, catalysis, batteries waste water treatment, sensors, drug delivery and curing dreadful diseases and many more, which has brought about the new, developing and exciting research field called nanoscience/nanotechnology which is driving of the new millennium.

Acknowledgements

The authors acknowledge the Royal Society-DFID Africa Capacity Building Initiative for their help and support. The authors also acknowledge the support received from the Enviromental Investment Fund (EIF) of Namibia: Matching fund subsidy from National Commission on Research Science and Technology (NCRST) for strengthening capacity at universities and research institutions in Namibia.

Conflict of interest

The authors of this chapter declare no conflict of interest.

Author details

Daniel Likius[1*], Ateeq Rahman[1*], Elise Shilongo[2] and Veikko Uahengo[1]

1 Department of Chemistry and Biochemistry, Faculty of Science, University of Namibia, Windhoek, Namibia

2 Department of Physics, Faculty of Science, University of Namibia, Windhoek, Namibia

*Address all correspondence to: daniels@unam.na and arahman@unam.na

References

[1] Li TM, Zeng W, Long HW, Wang ZC. Nanosheet-assembled hierarchical SnO_2 nanostructures for efficient gas-sensing applications. Actuators B. 2016;**231**:120-128

[2] Zeng Y, Wang TZ, Qiao L, Bing YF, Zou B, Zheng WTS. Synthesis and the improved sensing properties of hierarchical SnO_2 hollow nanosheets with mesoporous and multilayered interiors. Actuators B. 2016;**222**:354-361

[3] Eigler DM, Schweizer EK. Positioning single atoms with a scanning tunnelling microscope. Nature. 1990;**344**:524-526

[4] Heinrich AJ, Lutz CP, Gupta JA, Eigler DM. Molecule cascades. Science. 2002;**298**:1381-1387

[5] Brust M, Walker M, Bethell D, Schiffrin DJ, Whyman R. Synthesis of thiol-derivatised gold nanoparticles in a two-phase liquid–liquid system. Journal of the Chemical Society, Chemical Communications. 1994:801-802

[6] Kiely CJ, Fink J, Brust M, Bethell D, Schiffrin DJ. Spontaneous ordering of bimodal ensembles of nanoscopic gold clusters. Nature. 1998;**396**:444-446

[7] Zhang YF, Zheng JQ, Tao H, Tian F, Meng C. Synthesis and supercapacitor electrode of VO_2 (B)/C core–shell composites with a pseudocapacitance in aqueous solution. Applied Surface Science. 2016;**371**:189-195

[8] Su DZ, Zhao YJ, Yan D, Ding CH, Li JB, Jin HB. Enhanced composites of V_2O_5 nanowires decorating on graphene layers as ideal cathode materials for lithium-ion batteries. Journal of Alloys & Compounds. 2017;**695**:2974-2980

[9] Su DZ, Zhao YJ, Zhang RB, Zhao YZ, Zhou HP, Li JB, et al. Dimension meditated optic and catalytic performance over vanadium pentoxides. Applied Surface Science. 2017;**389**:112-117

[10] Wang NN, Zhang YF, Hu T. Facile hydrothermal synthesis of ultrahigh-aspect-ratio V_2O_5 nanowires for high-performance supercapacitors. Current Applied Physics. 2015;**15**:493-498

[11] Peng X, Zhang XM, Wang L, et al. Hydrogenated V_2O_5 nanosheets for superior lithium storage properties. Advanced Functional Materials. 2016;**26**:784-791

[12] Xu XM, Zhao YJ, Zhao YZ, Zhou HP, Rehman F, Li JB, et al. Self-assembly process of China rose-like β-$Co(OH)_2$ and its topotactic conversion route to Co_3O_4 with optimizable catalytic performance. CrystEngComm. 2015;**17**:8248-8256

[13] Shuquan L, Yang H, Zhiwei N, Han H, Tao C, Anqiang P, et al. Template-free synthesis of ultra-large V_2O_5 nanosheets with exceptional small thickness for high-performance lithium-ion batteries. Nano Energy. 2015;**13**:58-66

[14] Cheng J, Wang B, Xin HL, Yang G, Cai H, Nie F, et al. Self-assembled V_2O_5 nanosheets/reduced graphene oxide hierarchical nanocomposite as a high-performance cathode material for lithium ion batteries. Journal of Materials Chemistry A. 2013;**1**(36): 10814-10820

[15] Yang FC, Guo ZG. Engineering NiO sensitive materials and its ultra-selective detection of benzaldehyde. Journal of Colloid and Interface Science. 2016;**467**:192-202

[16] Chen X, Li C, Grätzel M, Kostecki R, Mao SS. Nanomaterials for renewable energy production and storage. Chemical Society Reviews. 2012;**41**:7909-7937

[17] Yang M, Tao QF, Zhang XC, Tang AD, Ouyang J. Solid-state synthesis and electrochemical property of SnO_2/NiO nanomaterials. Journal of Alloys and Compounds. 2008;**459**:98-102

[18] Jiang J, Handberg ES, Liu F, Liao YT, Wang HY, Li Z, et al. Effect of doping the nitrogen into carbon nanotubes on the activity of NiO catalysts for the oxidation removal of toluene. Applied Catalysis B: Environmental. 2014:160, 716-161, 721

[19] Bai M, Dai HX, Deng JG, Liu YX, Ji KM. Porous NiO nanoflowers and nanourchins: Highly active catalysts for toluene combustion. Catalysis Communications. 2012;**27**:148-153

[20] Gu L, Xie WH, Bai SA, Liu BL, Xue S, Li Q, et al. Facile fabrication of binder-free NiO electrodes with high rate capacity for lithium-ion batteries. Applied Surface Science. 2016;**368**:298-302

[21] Zhao F, Shao Y, Zha JC, Wang HY, Yang Y, Ruan SD, et al. Large-scale preparation of crinkly NiO layers as anode materials for lithium-ion batteries. Ceramics International. 2016;**42**:3479-3484

[22] Cui F, Wang C, Wu SJ, Liu G, Zhang FF, Wang TM. Lotus-root-like NiO nanosheets and flower-like NiO microspheres: Synthesis and magnetic properties. CrystEngComm. 2011;**13**:4930-4934

[23] Zhu P, Xiao HM, Liu XM, Fu SY. Template-free synthesis and characterization of novel 3D urchin-like α-Fe_2O_3 superstructures. Journal of Materials Chemistry. 2006;**16**:1794-1797

[24] Wang W, Zeng ZCW. Assembly of 2D nanosheets into 3D flower-like NiO: Synthesis and the influence of petal thickness on gas-sensing properties. Ceramics International. 2016;**42**:4567-4573

[25] Tian K, Wang XX, Li HY, Nadimicherla R, Guo X. Lotus pollen derived 3-dimensional hierarchically porous NiO microspheres for NO_2 gas sensing. Sensors and Actuators B: Chemical. 2016;**227**:554-560

[26] Lin LY, Liu TM, Miao B, Zeng W. Hydrothermal fabrication of uniform hexagonal NiO nanosheets: Structure growth and response. Materials Letters. 2013;**102-103**:43-46

[27] Lu Y, Ma YH, Ma SY, Jin WX, Yan SH, Xu XL, et al. Synthesis of cactus-like NiO nanostructure and their gas-sensing properties. Materials Letters. 2016;**164**:48-51

[28] Miao B, Zeng W, Lin LY, Xu S. Hydrothermal synthesis of nano sheets. Physica E. 2013;**52**:40-45

[29] Kumar R, Baratto C, Faglia G, Sberveglieri G, Bontempi E, Borgese L. Tailoring the textured surface of porous nanostructured NiO thin films for the detection of pollutant gases. Thin Solid Films. 2015;**583**:233-238

[30] Sta I, Jlassi M, Kandyla M, Hajji M, Koralli P, Krout F, et al. Surface functionalization of sol–gel grown NiO thin films with palladium nanoparticles for hydrogen sensing. International Journal of Hydrogen Energy. 2016;**41**:3291-3298

[31] Carnes C-L, Klabunde K-J. The catalytic methanol synthesis over nanoparticle metal oxide catalysts. Journal of Molecular Catalysis A. 2003;**194**:227-236

[32] Ralston D, Govek M, Graf C, Jones D-S, Tanabe K, Klabunde K-J, et al. Fuel processing nano particles. Fuel Processing Technology. 1978;**1**:143-146

[33] Pradhan B-K, Kyotani T, Tomita A. Nickel nanowires of 4 nm diameter in the cavity of carbon

nanotubes. Chemical Communications. 1999:1317-1318

[34] Park J et al. Monodisperse nanoparticles of Ni and NiO: Synthesis, characterization, self-assembled superlattices, and catalytic applications in the Suzuki coupling reaction. Advanced Materials. 2005;**17**:429-434

[35] Yan H, Blan C-F, Holland B-T, Parent M, Smyrl W-H, Stein A. A chemical synthesis of periodic macroporous NiO & metallic Ni. Advanced Materials. 1999;**11**:1003-1006

[36] Wang Y, Zhu Q, Zhang H. Carbon nanotube-promoted Co–Cu catalyst for highly efficient synthesis of higher alcohols from syngas. Chemical Communications. 2005:523-525

[37] Pang H, Lu Q, Li Y, Gao F. Facile synthesis of nickel oxide nanotubes and their antibacterial, electrochemical and magnetic properties. Chemical Communications. 2009:7542-7544

[38] Yang Q, Sha J, Ma X, Yang D. Synthesis of NiO nano wires by a sol gel process. Materials Letters. 2005;**59**:1967-1970

[39] Wang W, Liu Y, Xu C, Zheng C, Wang G. Synthesis of NiO nanorods by a novel simple precursor thermal decomposition approach. Chemical Physics Letters. 2002;**362**:119-122

[40] Song LX, Yang ZK, Teng Y, Xia J, Du P. Nickel oxide nanoflowers: Formation, structure, magnetic property and adsorptive performance towards organic dyes and heavy metal ions. Journal of Materials Chemistry A. 2013;**1**:8731-8736

[41] Baghbanzadeh M, Carbone L, Cozzoli PD, Kappe CO. Microwave-assisted synthesis of colloidal inorganic nanocrystals. Angewandte Chemie, International Edition. 2011;**50**:11312-11359

[42] Bilecka I, Niederberger M. Microwave chemistry for inorganic nanomaterials synthesis. Nanoscale. 2010;**2**:1358-1374

[43] Tang Z, Zhang Z, Wang Y, Glotzer SC, Kotov NA. Self-assembly of CdTe nanocrystals into free-floating sheets. Science. 2006;**314**:274-278

[44] Zhang Z, Tang Z, Kotov NAS, Glotzer C. Spontaneous CdTe alloy CdS transition of stabilizer-depleted CdTe nanoparticles induced by EDTA. Nano Letters. 2007;**7**:1670-1675

[45] Zeng W, Miao R, Gao Q. SDS-assisted hydrothermal synthesis of NiO flake-flower architectures with enhanced gas-sensing properties. Applied Surface Science. 2016;**384**:304-310

[46] Zeng W, Cao S, Long H, Zhang H. Hydrothermal synthesis of novel flower-needle NiO architectures: Structure, growth and gas response. Materials Letters. 2015;**159**:385-388

[47] Qiu J, Weng B, Zhao L, Chang C, Shi Z, Li X, et al. Nanoflakes NiO synthesis. Journal of Nanomaterials. 2014;**11**. Art I281461

[48] Wang ZL, Kong XY, Ding Y, Gao PX, Hughes WL, Yang RS, et al. Semiconducting and piezoelectric oxide nanostructures induced by polar surfaces. Advanced Functional Materials. 2004;**14**:943-956

[49] Illy B, Shollock BA, MacManus-Driscoll JL, Ryan MP. Electrochemical growth of ZnO nanoplates. Nanotechnology. 2005;**16**:320-324

[50] Palumbo M, Henley SJ, Lutz T, Stolojan V, Silva SRP. A fast sonochemical approach for the synthesis of solution processable ZnO rods. Journal of Applied Physics. 2008;**104**:074906-0749066